

Harmonic Analysis of Grid-Connected VSCs Controlled in the Stationary Frame: Disturbance Rejection, Resonant Controller Design and Limitations

André G. P. Alves^{✉1}, Laís F. Crispino^{✉2}, Marcello S. Neves^{✉2,3},
Cleiton M. Freitas^{✉1}, Luís G. B. Rolim^{✉2}, Robson F. S. Dias^{✉2}

¹Universidade do Estado do Rio de Janeiro, Departamento de Engenharia Elétrica, Rio de Janeiro - RJ, Brazil.

²Universidade Federal do Rio de Janeiro, Departamento de Engenharia Elétrica, Rio de Janeiro - RJ, Brazil.

³Centro Federal de Educação Tecnológica Celso Suckow da Fonseca, Angra dos Reis - RJ, Brazil.

e-mail: andre.alves@eng.uerj.br; laiscrispino@poli.ufrj.br; neves_marcello@poli.ufrj.br;
cleiton.freitas@uerj.br; rolim@poli.ufrj.br; dias@dee.ufrj.br.

ABSTRACT The increase in the penetration of inverter based renewable energy resources comes with several challenges. For one, the power quality can be cited as an issue due to the impact of the electronic devices in the grid voltage profile, which can cause harmonic disturbances and then affect all other installations nearby. Considering the issue previously described, this paper analyzes the effects of grid voltage harmonic disturbances in the operation of a grid-connected Voltage Source Converter (VSC) with current control in the stationary reference frame. A mathematical model is derived and validated both through simulations and experiments in order to associate the voltage harmonic magnitude disturbance with the respective current harmonic magnitude response from the grid-connected VSC. The model is also utilized to tune paralleled resonant controllers to mitigate the effect. Furthermore, the results and analyses highlight not only the effectiveness but also the limitations from the proposal.

KEYWORDS disturbance rejection model, grid-connected VSC, harmonics, power quality, resonant controllers.

I. INTRODUCTION

Power quality is a hot topic for grid-connected systems. In fact, harmonic distortion is considered as one of the most significant power quality problems due to the increase in the presence of nonlinear loads and large-scale inverter-based distributed generation (DG) units [1]. It is important to note that power quality issues can arise both from the inverter's side [2] as from the grid's side [3]. Moreover, if the voltages imposed by the grid are distorted, the currents generated by a new converter connected to that same grid can also be distorted, aggravating the issue. Such concern is seriously taken by the Distribution System Operators (DSOs) [4], which impose limits for current and voltage harmonics present in Point of Common Coupling (PCC). These requirements are also present in international standards such as IEEE Std 519-2022 [5], which are carefully considered by the literature [6] while detailing the issues caused at the inverter's side, as well as the respective solutions [3], [6].

Considering the focus in this particular topic, most papers found in the literature propose solutions to reduce the harmonic distortion content in the currents, however, the problem itself is not properly characterized. For instance, the study presented in [7] proposes a current harmonic

compensation technique through the implementation of a multi resonant controller. The strategy adopted by the authors is effective and was able to maintain the current's Total Demand Distortion (TDD) below the limits found in [5], however, the relationship between the harmonic voltage and the harmonic current was not investigated and the controllers were just tuned based in stability parameters. A performance comparison of harmonic mitigation schemes was conducted in [8], where the authors clearly show the effectiveness of utilizing resonant controllers through different implementation methodologies. The tuning of these controllers, however, only considered the stability margins of the control loop, which is not enough for the designer to establish how much current harmonic mitigation is going to be performed by the control system. The study shown in [9] also provides a control solution to mitigate the current harmonic distortion with a reduction in the transfer function order in comparison to the use of resonant controllers. The solution is effective in terms of harmonic cancellation, but the same issue is found where no mathematical model was utilized to tune the controller according to the harmonic mitigation. Only stability metrics are adopted during the controller design process.

The study presented in [10] proposed a fuzzy active disturbance rejection control where the parameters were self-tuned based in a nonlinear state error feedback control law, and the stability was guaranteed through a passivity methodology. On the other hand, such methodology did not allow a way for the user to determine the harmonic current of the system before the implementation, characterizing a limitation and a design issue. Holloweg et al. [11] proposed an adaptive controller for harmonic compensation that provided currents with smaller harmonic content in comparison to the classical multiresonant controller strategy at the cost of having a higher computational burden. Nevertheless, the authors stated that the fixed resonant controller gains were selected based in the experience of the designer and were not aimed for optimal performance. As such, it opens up a necessity for designing such gains through a methodology that considers harmonic current and voltage limitations during the design process. Finally, Alves et al. [12] proposed a methodology where both the current harmonic mitigation and stability are considered during the design process. However, the method was exemplified only for grid-connected VSCs controlled in the dq frame. As such, it is important to show how the methodology can be adapted for the cases where the current control is in the $\alpha\beta$ reference frame, since it is also commonly found in the literature for grid-connected applications [13]. Moreover, the limitations from the methodology were not discussed in the referenced paper, requiring further studies and theoretical analyses.

Considering the stated above, this paper proposes an adaptation of the method found in [12], where a disturbance rejection analysis is utilized for a grid-connected VSC, allowing the prediction of the VSC's output current harmonics according to the grid voltage harmonics and, finally, the design and implementation of resonant controllers to mitigate such phenomenon based in the desired harmonic level.

Furthermore, this study is an extension from the one published in [14], containing more theoretical analyses, simulation results, experiments to validate the methodology, and discussions regarding the limitations of the proposal. As such, the study has been significantly improved. In summary, the following contributions are now presented:

- Theory concepts now show how the disturbance rejection analysis can be associated with the VSC's admittance in the Laplace domain;
- The frequency responses are now detailed in order to show how the resonant controllers impact in the disturbance rejection model seen by the system;
- Design criteria is thoroughly detailed not only in terms of current harmonic limitation, which was already part of the contribution from [14], but also in terms of stability.
- Limitations from the proposed analysis are presented, thoroughly discussed, and also explain the situations where the methodology indicated more conservative or

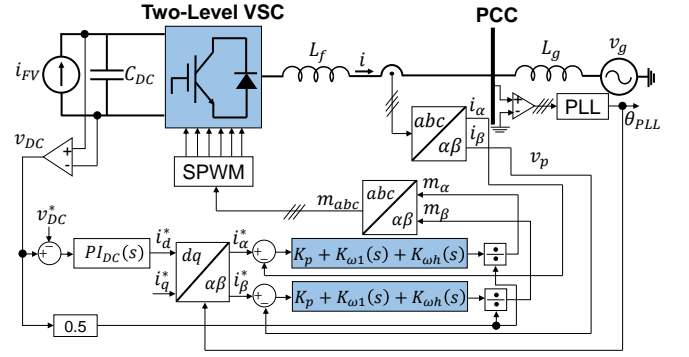


FIGURE 1. Grid-connected VSC controlled in the stationary reference frame.

innaccurate results, which was one of the future works recommended in [14].

II. THEORY CONCEPTS

A. Grid-connected VSC Dynamics and Control

Figure 1 shows the grid-connected VSC with the current control in the stationary reference frame, where the resonant controller $K_{\omega_1}(s)$ is adopted to regulate the current according to the references in the fundamental frequency to satisfy the desired active and reactive powers, and the resonant controller $K_{\omega_h}(s)$ is responsible for mitigating the undesirable current harmonic in a frequency multiple of the fundamental. In general, $K_{\omega_h}(s)$ can be expressed as:

$$K_{\omega_h}(s) = K_h \frac{2\omega_{B_h} s}{s^2 + 2\omega_{B_h} s + \omega_h^2}, \quad (1)$$

where it can be noted that the gain K_h is exactly the gain given by the controller at the tuned frequency ω_h . The bandwidth ω_{B_h} is commonly selected as a percentage of the tuned frequency [12].

The mathematical model associating the grid current and voltage can be obtained in the stationary reference frame as [15]:

$$v_{inv,\alpha} - v_{g,\alpha} = (L_f + L_g) \frac{di_\alpha}{dt}, \quad (2)$$

$$v_{inv,\beta} - v_{g,\beta} = (L_f + L_g) \frac{di_\beta}{dt}. \quad (3)$$

To adapt this model to the per unit system in the Laplace domain, the expressions can be divided by the base voltage v_b and base current i_b , noting that the base impedance is $Z_b = v_b/i_b$, and then applying the Laplace Transform:

$$\underline{V}_{inv,\alpha}(s) - \underline{V}_{g,\alpha}(s) = \frac{s(L_f + L_g)}{Z_b} \underline{I}_\alpha(s), \quad (4)$$

$$\underline{V}_{inv,\beta}(s) - \underline{V}_{g,\beta}(s) = \frac{s(L_f + L_g)}{Z_b} \underline{I}_\beta(s). \quad (5)$$

Figure 2 summarizes this model, noting that T_s is the sampling interval and $e^{-1.5sT_s}$ represents the delay associated

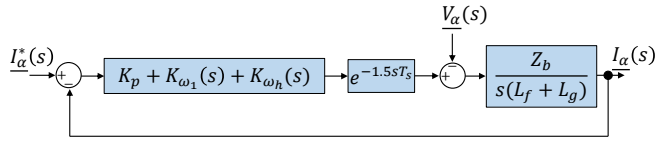


FIGURE 2. Block diagram highlighting the disturbance rejection dynamics in per unit.

with the converter's PWM and the controller's processing. Then, the effect of the grid voltage harmonics in the converter's output currents is represented by:

$$\frac{I_{\alpha}(s)}{V_{\alpha}(s)} = -\frac{\frac{Z_b}{sL_{eq}}}{1 + (K_p + K_{\omega_1}(s) + K_{\omega_h}(s))e^{-1.5sT_s} \frac{Z_b}{sL_{eq}}}, \quad (6)$$

$$\frac{I_{\alpha}(s)}{V_{\alpha}(s)} = -\frac{1}{\frac{sL_{eq}}{Z_b} + (K_p + K_{\omega_1}(s) + K_{\omega_h}(s))e^{-1.5sT_s}}, \quad (7)$$

where $L_{eq} = L_f + L_g$ is the equivalent inductance seen by the converter. Note that (7) evaluates the amount of harmonic current being outputted by the converter into the grid according to the voltage harmonic disturbance applied in the stationary reference frame.

By applying $s = j\omega_h$, considering that $\omega_h^2 \gg \omega_1^2$ into (1) and Euler's formula:

$$\frac{I_{\alpha}(j\omega_h)}{V_{\alpha}(j\omega_h)} = -\frac{1}{j\omega_h L_{eq}/Z_b + (K_p + K_h - j2K_1\omega_{B1}/\omega_h) \cdot (\cos(1.5\omega_h T_s) - j\sin(1.5\omega_h T_s))}. \quad (8)$$

Then, defining the grid harmonic voltage V_h and VSC output harmonic current I_h in percentages as:

$$V_h(\%) = 100\% \times |V_{\alpha}(j\omega_h)|, \quad (9)$$

$$I_h(\%) = 100\% \times |I_{\alpha}(j\omega_h)|, \quad (10)$$

and the angle θ_h as:

$$\theta_h = 1.5\omega_h T_s, \quad (11)$$

it is possible to take the magnitude from (8):

$$\frac{V_h(\%)}{I_h(\%)} = \left\{ \left[(K_p + K_h)\cos\theta_h - \frac{2K_1\omega_{B1}\sin\theta_h}{\omega_h} \right]^2 + \left[\frac{\omega_h L_{eq}}{Z_b} - \frac{2K_1\omega_{B1}\cos\theta_h}{\omega_h} - (K_p + K_h)\sin\theta_h \right]^2 \right\}^{1/2}, \quad (12)$$

which provides the following quadratic equation and solution, similarly to [12]:

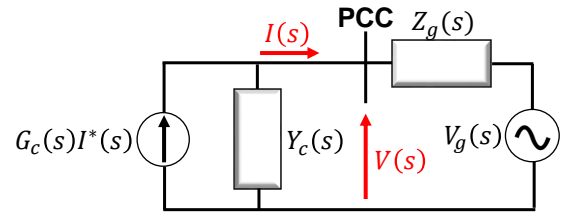


FIGURE 3. Equivalent system of the converter and the grid.

$$(K_p + K_h)^2 - 2\mu_1(K_p + K_h) + \mu_0 = 0, \quad (13)$$

$$K_h = -K_p + \mu_1 + \sqrt{\mu_1^2 - \mu_0}, \quad (14)$$

where:

$$\mu_1 = \frac{\omega_h L_{eq} \sin\theta_h}{Z_b}, \quad (15)$$

$$\mu_0 = \left(\frac{2K_1\omega_{B1}}{\omega_h} \right)^2 + \left(\frac{\omega_h L_{eq}}{Z_b} \right)^2 - \frac{4K_1\omega_{B1}L_{eq}\cos\theta_h}{Z_b} - \left(\frac{V_h(\%)}{I_h(\%)} \right)^2. \quad (16)$$

Equation (14) provides an analytical solution to calculate the resonant gain K_h that imposes the current harmonic $I_h(\%)$ according to the grid voltage harmonic $V_h(\%)$ for the system parameters.

B. Disturbance rejection model and VSC's admittance

The literature commonly adopts the Norton equivalent model to represent the converter behaviour [16], while representing the grid by its Thévenin equivalent model seen from the PCC. The transfer function $G_c(s)$ represents the closed-loop current control, which can be easily derived from Figure 2 as:

$$G_c(s) = \frac{(K_p + K_{\omega_1}(s) + K_{\omega_h}(s))e^{-1.5sT_s} \frac{Z_b}{s(L_f + L_g)}}{1 + (K_p + K_{\omega_1}(s) + K_{\omega_h}(s))e^{-1.5sT_s} \frac{Z_b}{s(L_f + L_g)}}. \quad (17)$$

On the other hand, $Y_c(s)$ represents the converter's admittance, which is a function of the converter's output filter and the embedded control loop being utilized in the application [17]. From Figure 3, Kirchhoff's Current Law (KCL) gives:

$$G_c(s)I^*(s) = Y_c(s)V(s) + I(s), \quad (18)$$

which can be written with the variables in per unit as:

$$G_c(s)\underline{I}^*(s)I_b = Y_c(s)\underline{V}(s)V_b + \underline{I}(s)I_b, \quad (19)$$

where V_b and I_b are, respectively, the voltage and current bases of the system. Dividing both members for I_b and noting that $Z_b = V_b/I_b$:

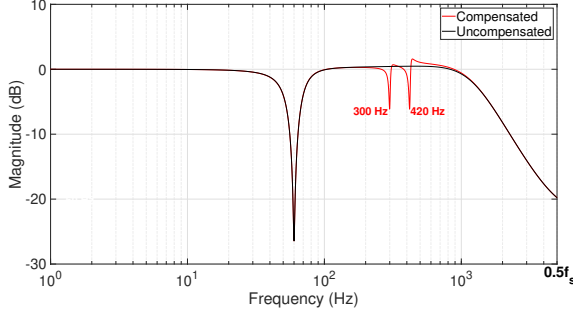


FIGURE 4. Magnitude response of the disturbance rejection model from (8) with and without resonant compensators.

$$G_c(s)\underline{I}^*(s) = Y_c(s)\underline{V}(s)Z_b + \underline{I}(s), \quad (20)$$

$$Y_c(s) = \frac{G_c(s)\underline{I}^*(s)}{Z_b\underline{V}(s)} - \frac{1}{Z_b}\frac{\underline{I}(s)}{\underline{V}(s)}, \quad (21)$$

and, as a consequence, the following definitions are derived:

$$Y_c(s) = -\frac{1}{Z_b}\frac{\underline{I}(s)}{\underline{V}(s)}\Bigg|_{\underline{I}^*(s)=0}. \quad (22)$$

$$Y_c(s) = -\frac{\underline{I}(s)}{\underline{V}(s)}\Bigg|_{\underline{I}^*(s)=0}. \quad (23)$$

It can be noted that the converter's admittance $Y_c(s)$ can be obtained through the disturbance rejection model from (7). Of course, since the voltage in this case is the PCC voltage, only the VSC output filter impedance should be utilized, rather than the equivalent from the filter and grid. The minus signal contained in (23) is, of course, due to the orientation of the current $\underline{I}(s)$ in Figure 3.

By considering the system from Figure 1 and the parameters contained in Table 1, the magnitude response of the disturbance rejection model from (8) can be seen in Figure 4, with and without the resonant compensators.

C. Stability Analysis

In order to verify the stability of the system, it is possible to evaluate the frequency response from the open loop reference tracking transfer function $\underline{I}_\alpha(s)/\underline{I}_\alpha^*(s)$ obtained through Figure 2. Then, following the common strategies found in the literature, Bode and Nyquist plots are utilized to check the system stability.

Utilizing the parameters from Table 1, considering the fundamental controller and the resonant compensators from 300 Hz and 420 Hz, the Nyquist and Bode plots can be seen in Figures 5 and 6, respectively. In the Nyquist plot, it can be noted that the point (-1,0) is not encircled, guaranteeing that the system is closed-loop stable. Through the Bode plot, the stability margins are highlighted, indicating that the system presents a phase margin of 53.5° and a gain margin of 9.15 dB, which are in agreement with the recommended values found in the literature [18].

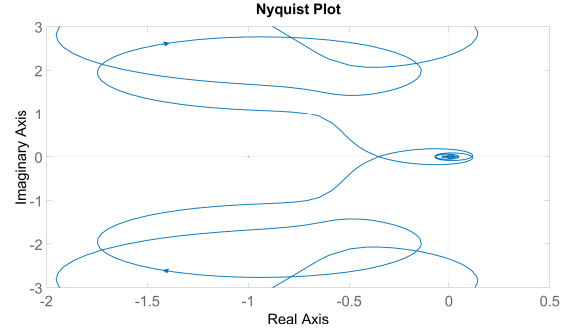


FIGURE 5. Nyquist plot indicating the stability of the system with the resonant controllers.

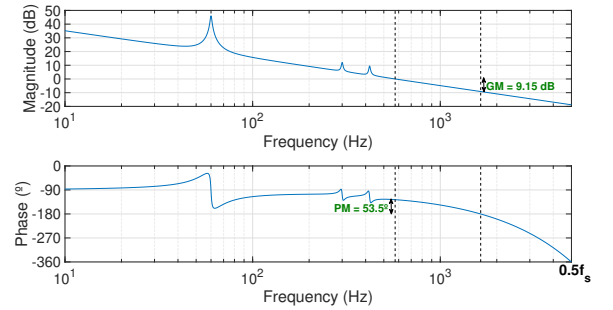


FIGURE 6. Open loop frequency response of the system with the resonant controllers.

Note that this stability evaluation is not, by any means, a novelty introduced by this work. It is just a necessary step in order to verify if the closed-loop system can be implemented and then tested with a functional control loop. The main contribution of this work is contained in the disturbance rejection model and its analyses, which can be utilized for prediction and also resonant controller design in terms of harmonic current mitigation in the stationary reference frame.

D. Non-linear effects disregarded by the model

This section aims at evaluating non-linear effects not covered by the provided model. This analysis is important in understanding some of the results that will be presented in Section III. At first, considering that the PCC voltage contains both a fundamental and a h-order negative sequence harmonic component while assuming the power invariant transformation from [19]:

$$v_\alpha(t) = \sqrt{3}V_1 \sin(\omega_1 t) + \sqrt{3}V_h \sin(h\omega_1 t + \phi_{v,h}), \quad (24)$$

$$v_\beta(t) = -\sqrt{3}V_1 \cos(\omega_1 t) + \sqrt{3}V_h \cos(h\omega_1 t + \phi_{v,h}). \quad (25)$$

The previous idea can be extended in order to express the VSC current in terms of two components, considering fundamental currents in phase with fundamental voltages, as follows:

$$i_\alpha(t) = \sqrt{3}I_1 \sin(\omega_1 t) + \sqrt{3}I_h \sin(h\omega_1 t + \phi_{i,h}), \quad (26)$$

$$i_\beta(t) = -\sqrt{3}I_1 \cos(\omega_1 t) + \sqrt{3}I_h \cos(h\omega_1 t + \phi_{i,h}). \quad (27)$$

Notice that I_h will tend to zero only if the harmonic component of $v_{inv,\alpha}$ and $v_{inv,\beta}$ match its counterpart (24) and (25).

In this condition, according to the pq theory [19], there are real and imaginary oscillating powers with a frequency equal to $(h+1)\omega_1$. In general, these oscillating powers will present two components, one due to the interaction between the fundamental current and the h-order voltage, and another due to the interaction of the h-order current with the fundamental voltage:

$$\begin{aligned} \tilde{p}(t) = & -3I_1 V_h \cos \left[(h+1)\omega_1 t + \phi_{v,h} \right] \\ & - 3I_h V_1 \cos \left[(h+1)\omega_1 t + \phi_{i,h} \right], \quad (28) \end{aligned}$$

$$\begin{aligned} \tilde{q}(t) = & 3I_1 V_h \sin \left[(h+1)\omega_1 t + \phi_{v,h} \right] \\ & - 3I_h V_1 \sin \left[(h+1)\omega_1 t + \phi_{i,h} \right]. \quad (29) \end{aligned}$$

In the same way, there will be oscillating power components at the AC terminals of the inverter. The difference here is that the converter has two groups of terminals, one AC and another DC, and because of the law of conservation of energy, the real power should be equal in both, if the converter losses are neglected. The direct consequence is that the DC voltage and DC current will present oscillating components with the same frequency of $\tilde{p}(t)$, i.e., $(h+1)\omega_1$. During the process of modulation, the converter transforms the DC voltage into AC according to:

$$v_{inv,\alpha}(t) = \frac{1}{2}v_{DC}(t)m_\alpha(t), \quad (30)$$

$$v_{inv,\beta}(t) = \frac{1}{2}v_{DC}(t)m_\beta(t), \quad (31)$$

where m_α and m_β are the modulation indices. The fundamental components of these indices interact with the oscillating component of $v_{DC}(t)$, producing two harmonic components, one with negative sequence and frequency $h\omega_1$, and another with positive sequence and frequency $(h+2)\omega_1$. It goes without saying that the converter introduces new harmonic components into the system.

Notice that this introduction of harmonic content cannot be prevented by mitigating the oscillation in v_{DC} , nor in any other mean. An oscillation-free v_{DC} , for instance, would pave the way for increasing the oscillations in i_{DC} , since $\tilde{p}_{DC} = \tilde{p}(t)$. In this case, the DC-transformer analogy [20] can be utilized to write the relationship between AC and DC currents in an inverter:

$$i_{DC} = \frac{1}{2}m_\alpha i_\alpha + \frac{1}{2}m_\beta i_\beta. \quad (32)$$

Once more, the $(h+1)$ -order component in i_{DC} can only be obtained if i_α and i_β contain components with the frequencies $h\omega_1$ and $(h+2)\omega_1$. In other words, the mechanism changes, yet the harmonic introduction continues.

There is also a second mechanism of harmonic introduction in the grid, and it occurs when the inverter is compensating some harmonic component. According to [19], when the converter compensates a specific harmonic component, it inherently creates hidden currents/voltages. For instance, a negative-sequence 5th-harmonic compensation leads to 7th-order hidden currents with a positive sequence. In general, the hidden harmonics tend to be canceled when the oscillating powers \tilde{p} and \tilde{q} are proportionally compensated. Notice that the proportional compensation makes the amplitudes of \tilde{p} and \tilde{q} remain equal. Conversely, if \tilde{p} and \tilde{q} are not proportionally compensated, their amplitudes will not be equal, and the converter will output small, non-desired, harmonic components. To better understand this aspect, we can divide the $\alpha\beta$ currents into two components, one associated to the real power and the another with the imaginary power [19, Sec. 3.2.2.A], as follows:

$$i_\alpha = \frac{v_{inv,\alpha}}{v_{inv,\alpha}^2 + v_{inv,\beta}^2} \tilde{p}_{inv} + \frac{v_{inv,\beta}}{v_{inv,\alpha}^2 + v_{inv,\beta}^2} \tilde{q}_{inv}, \quad (33)$$

$$i_\beta = \frac{v_{inv,\beta}}{v_{inv,\alpha}^2 + v_{inv,\beta}^2} \tilde{p}_{inv} - \frac{v_{inv,\alpha}}{v_{inv,\alpha}^2 + v_{inv,\beta}^2} \tilde{q}_{inv}. \quad (34)$$

When the inverter is set to compensate a h-order negative-sequence harmonic component, it produces \tilde{p}_{inv} and \tilde{q}_{inv} accordingly. In this case, if we disregard the harmonic components in the voltage for the sake of simplicity, the converter will produce the following currents:

$$\begin{aligned} i_\alpha = & \sqrt{3}I_h \sin(h\omega_1 t) - \frac{\sqrt{3}}{2}I_{h+2,p} \sin((h+2)\omega_1 t) \\ & + \frac{\sqrt{3}}{2}I_{h+2,q} \sin((h+2)\omega_1 t), \quad (35) \end{aligned}$$

$$\begin{aligned} i_\beta = & \sqrt{3}I_h \cos(h\omega_1 t) + \frac{\sqrt{3}}{2}I_{h+2,p} \cos((h+2)\omega_1 t) \\ & - \frac{\sqrt{3}}{2}I_{h+2,q} \cos((h+2)\omega_1 t). \quad (36) \end{aligned}$$

If the amplitudes of \tilde{p}_{inv} and \tilde{q}_{inv} are equal, then $I_{h+2,p} = I_{h+2,q} = I_h$, and the currents will only contain the h-order harmonic component. Conversely, the inverter will introduce the $(h+2)$ -order harmonic component in the output current.

Note that the current control utilized in Figure 1 aims at reducing the magnitude of specific harmonic current components, yet it does not guarantee proportional compensation of the terms \tilde{p} and \tilde{q} associated with these harmonics. In short, the proportional compensation depends on the produced harmonic voltage being in phase with the corresponding harmonic voltage of the grid. This, indeed, would require extra control loops, compromising the simplicity of the mitigation approach. The phasor diagrams in Fig. 7 are inspired by the idea conveyed by (33) and (34), i.e., the voltage components in the x and y axes are proportional to real and imaginary powers. Fig. 7(a) shows the case where there is proportional compensation, thus:

$$\frac{v_{inv,h,p}}{v_{h,p}} = \frac{v_{inv,h,q}}{v_{h,q}}. \quad (37)$$

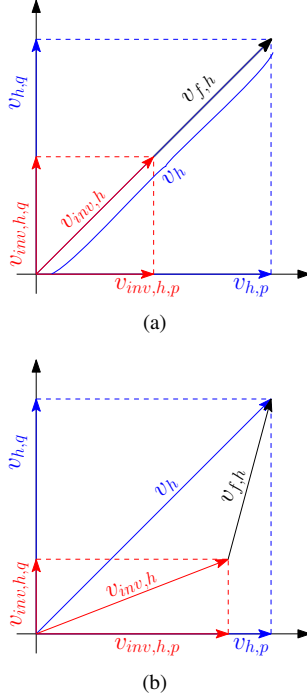


FIGURE 7. Phasor diagram for (a) Proportional, (b) disproportional compensation of p_h and q_h .

When the result in (37) does not hold, we have the disproportional condition portrayed in Fig. 7(b). It is important to notice that the harmonic current is proportional to the voltage across the coupling inductor, $v_{f,h} = v_h - v_{inv,h}$. Once $v_{inv,h,p} \neq v_{inv,h,q}$, the amplitude of the oscillating real and active components will not be equal, and as a consequence, the inverter will introduce harmonics with frequency equal to $(h+2)\omega_1$, according to (35) and (36). Note that the presence of this component is also a consequence of a $(h+1)\omega_1$ component in the DC link voltage due to the existence of \tilde{p} , which will also affect the magnitude of the VSC h -order harmonics due to the modulation process according to (30) and (31).

III. APPLICATION EXAMPLE

The system from Figure 1 was simulated with PSIM, considering the parameters from Table 1. The controllers K_p and $K_{\omega_1}(s)$, responsible for the reference tracking in 60 Hz, were tuned based in the Naslin Polynomial method shown in [21]. The controllers $K_{\omega_5}(s)$ and $K_{\omega_7}(s)$, responsible for mitigating the current components in 300 Hz and 420 Hz, were tuned based in the proposed methodology summarized in the previous section and calculated through (14). All controllers were designed with a bandwidth ω_{B_h} around 1% of the respective tuned frequency [22]. Furthermore, the design details regarding the current harmonic limitations according to the voltage harmonic disturbances are going to be presented in the following subsections.

TABLE 1. Parameters for the grid-connected VSC controlled in the $\alpha\beta$ frame.

Parameter	Value
L_f	1.0 mH
L_g	1.5 mH
Sampling Frequency	10 kHz
i_{FV}	13.5 A
K_p	1.0
$K_{\omega_1}(s)$	$150.8s/(s^2 + 7.54s + 1.42 \times 10^5)$
$K_{\omega_5}(s)$	$41.51s/(s^2 + 37.7s + 3.55 \times 10^6)$
$K_{\omega_7}(s)$	$62.52s/(s^2 + 52.78s + 6.96 \times 10^6)$
f_g	60 Hz
V_g	$127\sqrt{2}$ V (peak/phase)
I_g	20 A (peak/phase)
Z_b	8.98 Ω
V_{DC}	400 V
$PI_{DC}(s)$	$10(1 + 60/s)$
PLL Bandwidth	110 Hz

A. 5th HARMONIC PREDICTION AND MITIGATION

In this case, the K_5 from the controller $K_{\omega_5}(s)$ was calculated through (14) with a design criterion of approximately 1% harmonic current $I_5(\%)$ for a 2% voltage harmonic disturbance $V_5(\%)$, resulting in $K_5 = 1.10$.

The three-phase currents obtained throughout the simulations and their harmonic spectrum, as well as the predicted current harmonics according to (12), can be seen in Figures 8 and 9. The first result shows the system without the implementation of $K_{\omega_5}(s)$, characterizing a current harmonic in 300 Hz of 2.0%, whereas the prediction would be 2.10%. The relative error for such prediction was 4.89%. The second result shows the implementation of $K_{\omega_5}(s)$, where a 1.08% harmonic current was observed, whereas the predicted value would be 1.0%, characterizing a relative error of 8.16%, which are indicators of agreement between the simulations and the disturbance rejection model.

B. 7th HARMONIC PREDICTION AND MITIGATION

The design criterion in this case was approximately a 0.5% harmonic current $I_7(\%)$ for a 1% voltage harmonic disturbance $V_7(\%)$, resulting in $K_7 = 1.18$.

The simulation results and predictions for the case without the implementation of the resonant controller can be seen in Figure 10, where the simulated currents presented a harmonic current of 0.93% in comparison to the prediction of 1.05%. A relative error of 13.7% was observed. The result and prediction with the resonant controller $K_{\omega_7}(s)$ can be seen in Figure 11. In this case, a harmonic current of 0.512% was observed during the simulations, whereas the design criterion was 0.5%, resulting in a relative error of 1.83%, also indicating that the methodology provides satisfactory results for designing resonant controllers.

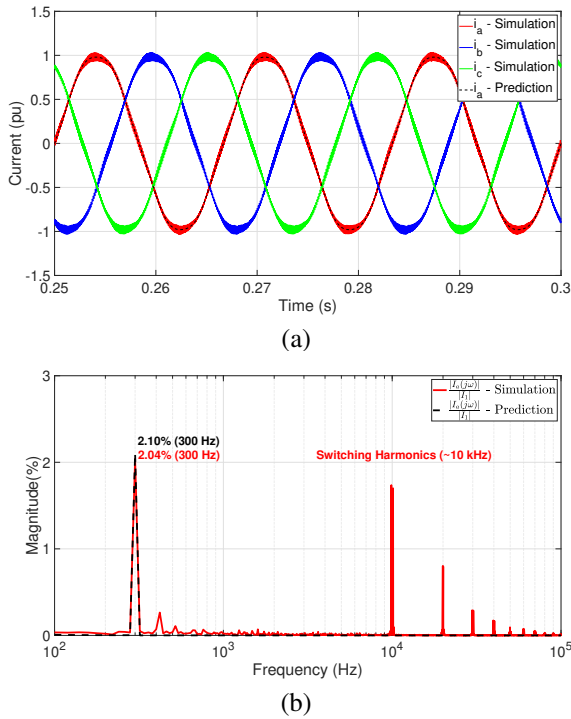


FIGURE 8. (a) current waveforms and (b) current harmonic spectrum for the simulated 2% voltage harmonic disturbance in 300 Hz without a resonant controller.

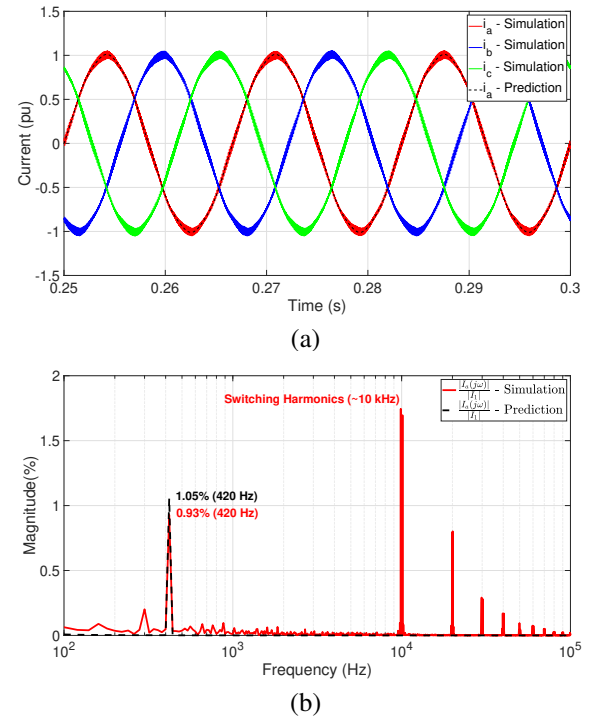


FIGURE 10. (a) current waveforms and (b) current harmonic spectrum for the simulated 1% voltage harmonic disturbance in 420 Hz without a resonant controller.

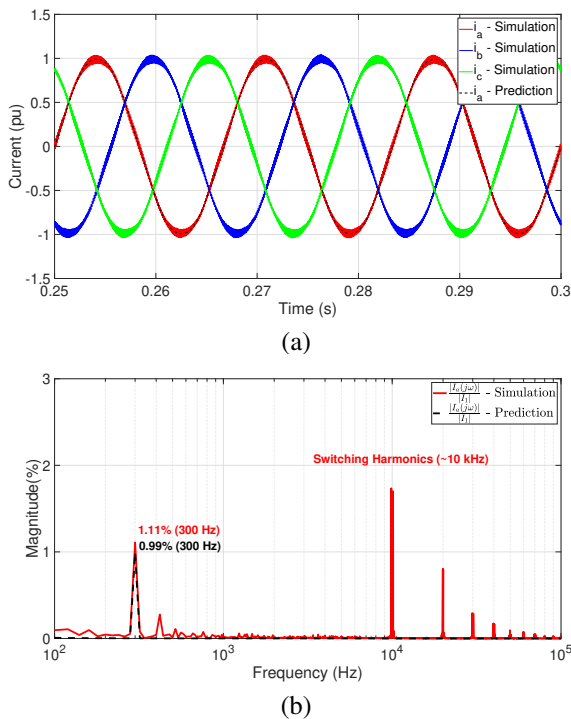


FIGURE 9. (a) current waveforms and (b) current harmonic spectrum for the simulated 2% voltage harmonic disturbance in 300 Hz with the implementation of K_{ω_g} .

An interesting aspect that can be seen from Figures 8(b) up to 11(b) is that there are other frequency components with

much smaller magnitudes around the harmonic under study, which are associated with the effects detailed in Section II D. The next section will further highlight and discuss the hidden currents' effects and their influences for the system.

C. Discussions Associated with the Hidden Currents

All of the results presented so far showed that the analytical model approaches the behavior of the controlled system for the 5th and 7th harmonic components. However, the appearance of hidden currents, as theoretically detailed in Section II D, may cause a mismatch between the disturbance rejection model and the results. Figures 8 and 10 also show that this effect occurs even without harmonic compensation.

The effects of the hidden harmonics increase with the magnitude of the oscillating power, and it is more noticeable at higher-order components, such as the 11th harmonic. For instance, Figure 12 indicates that the prediction of the 7th-order harmonic voltage by the disturbance rejection model agrees with the simulation results for all disturbances under study. Nonetheless, the increasing 7th-order disturbance causes an increasing 5th-order hidden current, as observed in Figure 13, which is not predicted by the linear model. This is not a significant issue, since it barely reaches 0.005pu for the highest voltage disturbance. For the sake of comparison, the hidden current changes the output current's Total Harmonic Disturbance (THD) from 2.50% to 2.55%, at the highest voltage disturbance. As previously mentioned, the negative effect is more noticeable at higher frequencies, such as when

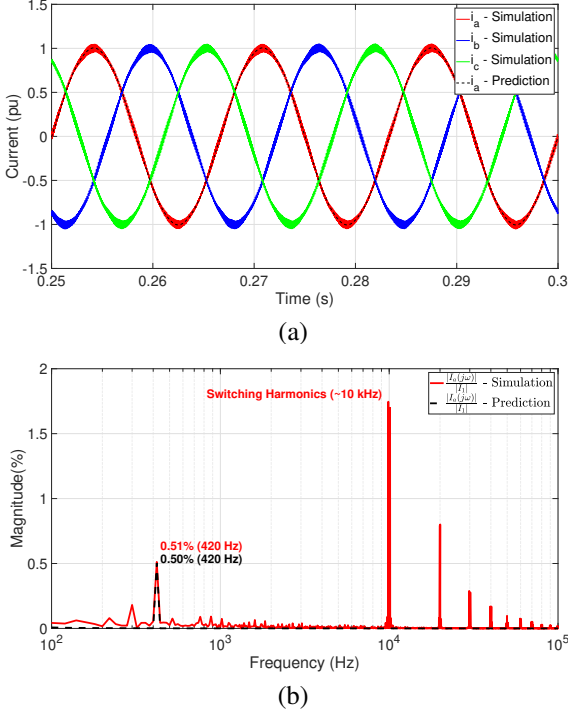


FIGURE 11. (a) current waveforms and (b) current harmonic spectrum for the simulated 1% voltage harmonic disturbance in 420 Hz with the implementation of $K_{\omega_7}(s)$.

dealing with the 11th-order disturbance. In this case, the prediction given by the disturbance rejection model was higher than the simulation result, as observed in Figure 14. This error, nonetheless, did not represent a significant issue, since the magnitude from the harmonic current in the simulation was smaller than the prediction, which could be considered as a conservative approach, specially during the design of resonant controllers. The discussions regarding this topic are important to motivate future works to improve the model and consider such effect.

IV. Experimental Results

In order to verify the previous analyses, experiments were conducted utilizing the real-time simulator Typhoon HIL

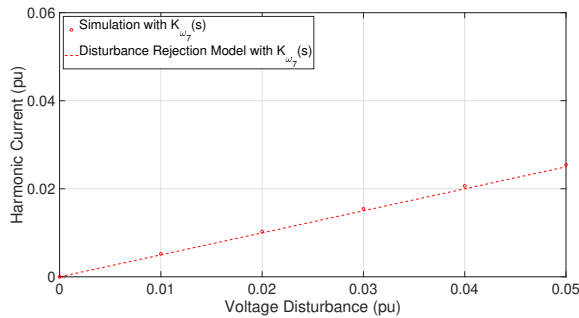


FIGURE 12. Comparison between the disturbance rejection analysis and the simulations for the 7th harmonic case with compensation.

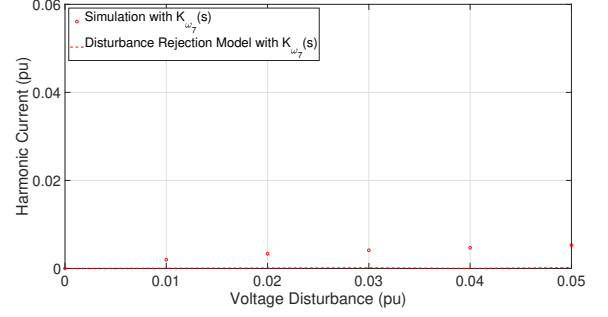


FIGURE 13. 5th harmonic hidden currents effect on the prediction of the disturbance rejection model in comparison to the simulations for the 7th harmonic case with compensation.

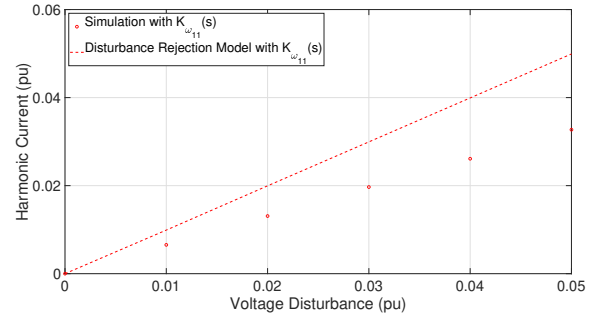


FIGURE 14. Comparison between the disturbance rejection analysis and the simulations for the 11th harmonic case with compensation.

602+, where both the grid and converter were modeled, the Digital Signal Processor (DSP) TMSF28379D, where the VSC control loop was embedded through digital implementation through Code Composer Studio, and the Yokogawa DL850EV oscilloscope for the data acquisition. The parameters adopted for the system are the same as the ones contained in Table 1. Furthermore, the testbed can be seen in Figure 15, noting that the DSP reads the current and voltage measurements from the real-time simulator at each sampling cycle, and then generates the PWM signals after the digital processing, which are then provided for the converter modelled within the real-time simulation executed by the HIL device.

Voltage harmonic disturbances from 2% up to 5% were applied during the experiment, firstly in 300 Hz, and secondly in 420 Hz. The objective was to compare the experimental results with the predictions from the disturbance rejection analysis from Section II, since it was utilized to design the resonant controllers.

Figures 16 and 17 show, respectively, the three-phase currents captured with the oscilloscope for the 300 Hz and 420 Hz voltage harmonic disturbances, respectively. Furthermore, the frequency spectrum for each situation along with the comparison between the experiment and the predictions from the disturbance rejection model can be seen in Figures 18, for the 300 Hz disturbance, and 19, for the 420 Hz disturbance. It is worth mentioning that the minimum and maximum current

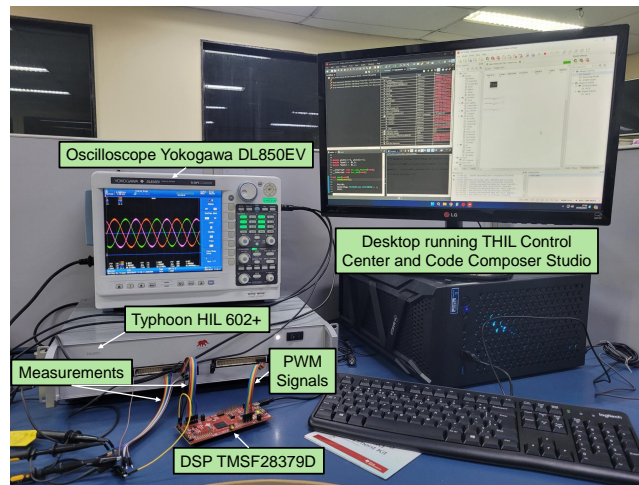


FIGURE 15. Testbed utilized to validate the proposal.

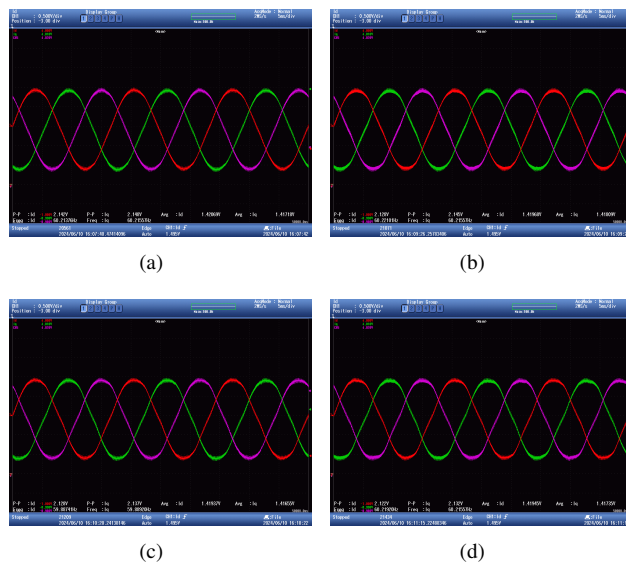


FIGURE 16. Three-phase currents for voltage harmonic disturbances for (a) 2%, (b) 3%, (c) 4%, (d) 5% in 300 Hz with compensation.

THD levels for the disturbances in 300 Hz were 1.54% and 2.98%, while for the disturbances in 420 Hz were 1.58% and 3.22%, which are below the limits established in [5].

Table 2 also highlights the comparison between the predictions and experimental results, both for the fifth as for the seventh harmonic disturbances. For the fifth harmonic disturbance case, relative errors between 11.1% and 28.2% were observed, with an average error of 16.9%, while for the seventh harmonic disturbance case, relative errors between 20.0% and 33.1% were observed, with an average error of 25.4%. Note that the highest relative errors are associated with the smallest voltage harmonic disturbances, which is justified by the fact that the error is put as percentage in the basis of a smaller prediction, increasing the ratio even for small deviations.

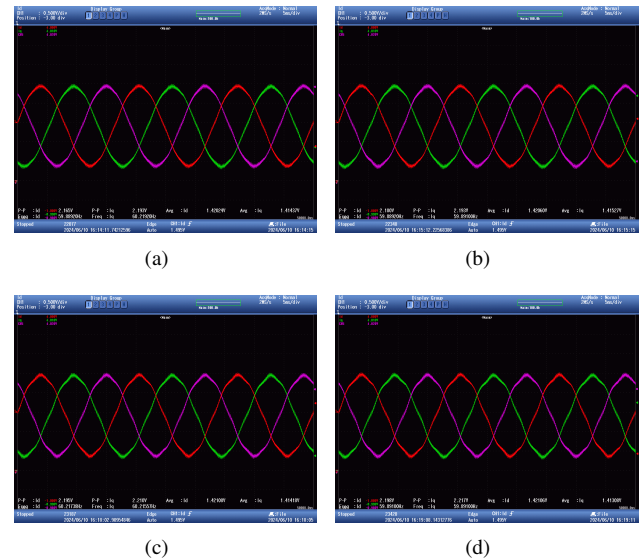


FIGURE 17. Three-phase currents for voltage harmonic disturbances for (a) 2%, (b) 3%, (c) 4%, (d) 5% in 420 Hz with compensation.

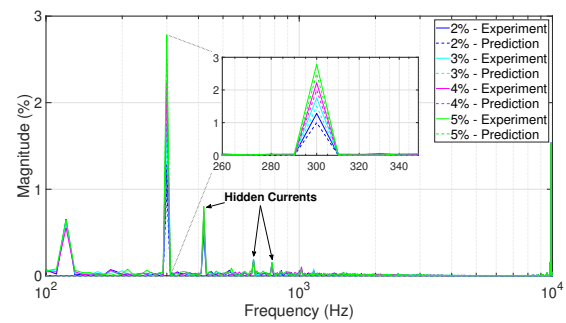


FIGURE 18. Three-phase currents' frequency spectrum for each voltage harmonic disturbance in 300 Hz with compensation.

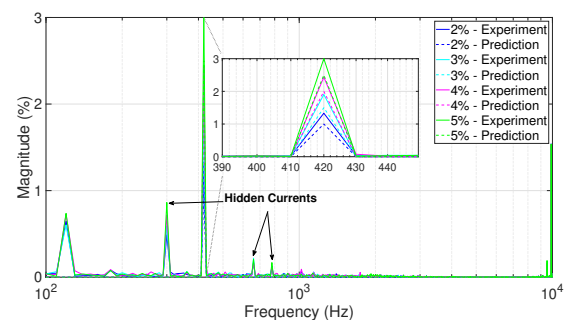


FIGURE 19. Three-phase currents' frequency spectrum for each voltage harmonic disturbance in 420 Hz with compensation.

In both cases, the proposed methodology was useful in order to design the resonant controllers according to desired current harmonic levels. However, the presence of the hidden harmonic currents, which are not considered in the disturbance rejection model utilized in this paper, affect the accuracy of the prediction, as also explained previously.

TABLE 2. Tabulation from the predicted and experimental results for the 300 Hz and 420 Hz harmonic disturbances with compensation.

Voltage Disturbance (%)	Predicted Current (%)	Experimental Current (%)	Relative Error (%)
300 Hz			
2,00	1,00	1,28	28,23
3,00	1,50	1,76	17,04
4,00	2,00	2,22	11,07
5,00	2,50	2,78	11,37
420 Hz			
2,00	1,00	1,33	33,12
3,00	1,50	1,90	26,89
4,00	2,00	2,44	21,83
5,00	2,50	3,00	20,04

Future studies can be conducted to improve the model and consider such effect.

V. CONCLUSIONS

The proposal of predicting the harmonic currents due to voltage harmonic disturbances was validated in the $\alpha\beta$ frame through simulations. A methodology capable of tuning resonant controllers based in such disturbance rejection model in the stationary reference frame was proposed and validated through simulations and experiments.

It was shown that hidden harmonic currents can appear due to the oscillating powers exchanged with the grid, creating a mismatch between the disturbance rejection model and the results. As previously discussed, this effect creates a limitation in the proposal that can be further investigated and mitigated in future studies. However, the methodology presented in this paper can still be utilized for designing resonant controllers as a conservative approach.

ACKNOWLEDGEMENTS

This study was financed in part by the Coordenação de Aperfeiçoamento de Pessoal de Nível Superior - Brasil (CAPES) - Finance Code 001 and also by Instituto Nacional de Energia Elétrica (INERGE)

AUTHOR CONTRIBUTIONS

ALVES, A.G.P.: Conceptualization, Data Curation, Formal Analysis, Investigation, Methodology, Project Administration, Software, Supervision, Validation, Visualization, Writing – Original Draft, Writing – Review & Editing. **CRISPINO, L.F.:** Data Curation, Formal Analysis, Investigation, Methodology, Software, Validation, Visualization, Writing – Review & Editing. **NEVES, M.S.:** Data Curation, Investigation, Resources, Software, Validation, Visualization, Writing – Review & Editing. **FREITAS, C.M.:** Data Curation, Formal Analysis, Investigation, Methodology, Visualization, Writing – Review & Editing. **ROLIM, L.G.B.:** Conceptualization, Formal Analysis, Funding Acquisition,

Methodology, Resources, Supervision, Writing – Original Draft. **DIAS, R.F.S.:** Conceptualization, Funding Acquisition, Resources, Supervision, Writing – Original Draft.

PLAGIARISM POLICY

This article was submitted to the similarity system provided by Crossref and powered by iThenticate – Similarity Check.

REFERENCES

- [1] S. H. E. Abdel Aleem, A. F. Zobaa, M. E. Balci, S. M. Ismael, "Harmonic Overloading Minimization of Frequency-Dependent Components in Harmonics Polluted Distribution Systems Using Harris Hawks Optimization Algorithm", *IEEE Access*, vol. 7, pp. 100824–100837, 2019, doi:10.1109/ACCESS.2019.2930831.
- [2] M. G. Joksimović, L. S. Perić, S. N. Vukosavić, "Closed-Loop Harmonic Suppression for Grid Connected 3-Phase PWM Inverters", *IEEE Transactions on Power Electronics*, vol. 39, no. 2, pp. 2677–2691, 2024, doi:10.1109/TPEL.2023.3332819.
- [3] B. Yang, H. Li, L. Shan, L. Wei, S. Lu, "A Fundamental and Harmonic Frequencies Decoupled Control Scheme to Improve the Output Current Quality of Grid-forming Inverters", *IEEE Transactions on Power Electronics*, pp. 1–13, 2024, doi:10.1109/TPEL.2024.3416469.
- [4] M. Bajaj, A. K. Singh, "Grid integrated renewable DG systems: A review of power quality challenges and state-of-the-art mitigation techniques", *International Journal of Energy Research*, vol. 44, no. 1, pp. 26–69, 2020, doi:https://doi.org/10.1002/er.4847.
- [5] "IEEE Standard for Harmonic Control in Electric Power Systems", *IEEE Std 519-2022 (Revision of IEEE Std 519-2014)*, pp. 1–31, 2022, doi:10.1109/IEEESTD.2022.9848440.
- [6] P. Kalkal, A. V. R. Teja, "A Novel Graphical Technique for Multiple Harmonic Mitigation in a Two-Level Inverter With Only Two Switching Angles", *IEEE Journal of Emerging and Selected Topics in Power Electronics*, vol. 12, no. 3, pp. 3052–3062, 2024, doi:10.1109/JESTPE.2024.3380576.
- [7] S. Srita, S. Somkun, "Implementation of Harmonic Compensation for Three-Phase Grid-Connected Voltage-Source Converter Under Grid Voltage Distortion", in *2022 19th International Conference on Electrical Engineering/Electronics, Computer, Telecommunications and Information Technology (ECTI-CON)*, pp. 1–5, 2022, doi:10.1109/ECTI-CON54298.2022.9795533.
- [8] S. Srita, S. Somkun, "Implementation and performance comparison of harmonic mitigation schemes for three-phase grid-connected voltage-source converter under grid voltage distortion: HiL and experimental validation", *AEU - International Journal of Electronics and Communications*, vol. 161, p. 154552, 2023, doi:https://doi.org/10.1016/j.aeue.2023.154552, URL: https://www.sciencedirect.com/science/article/pii/S1434841123000262.
- [9] H. Gholizade-Narm, S. A. Khajehoddin, M. Karimi-Ghartemani, "Reduced-Order Controllers Using Integrated Controller-Plant Dynamics Approach for Grid-Connected Inverters", *IEEE Transactions on Industrial Electronics*, vol. 68, no. 8, pp. 7444–7453, 2021, doi:10.1109/TIE.2020.3007119.
- [10] H. Yan, H. Cai, "Research on Fuzzy Active Disturbance Rejection Control of LCL Grid-Connected Inverter Based on Passivity-Based Control in Weak Grid", *Electronics*, vol. 12, no. 8, 2023, doi:10.3390/electronics12081847, URL: https://www.mdpi.com/2079-9292/12/8/1847.
- [11] G. V. Hollweg, P. J. D. d. O. Evald, E. Mattos, L. C. Borin, R. V. Tambara, H. A. Gründling, W. Su, "A Direct Adaptive Controller With Harmonic Compensation for Grid-Connected Converters", *IEEE Transactions on Industrial Electronics*, vol. 71, no. 3, pp. 2978–2989, 2024, doi:10.1109/TIE.2023.3270535.
- [12] A. G. P. Alves, L. G. B. Rolim, R. F. d. S. Dias, J. d. S. Ramos, "Analysis of Grid-Connected VSCs Subject to Voltage Harmonic Disturbances: Prediction and Design Tool of Resonant Controllers", *IEEE Transactions on Energy Conversion*, vol. 38, no. 1, pp. 239–249, 2023, doi:10.1109/TEC.2022.3196244.
- [13] I. D. L. Costa, D. I. Brandao, L. Matakas Junior, M. G. Simões, L. M. F. Morais, "Analysis of Stationary- and Synchronous-Reference Frames for Three-Phase Three-Wire Grid-Connected Converter AC Current Regulators", *Energies*, vol. 14, no. 24, 2021,

- doi:10.3390/en14248348, URL: <https://www.mdpi.com/1996-1073/14/24/8348>.
- [14] A. G. P. Alves, R. F. S. Dias, L. G. B. Rolim, “Disturbance Rejection Analysis of Grid-Connected VSCs Controlled in the Stationary Reference Frame Under Voltage Harmonic Disturbances”, in *2023 IEEE 8th Southern Power Electronics Conference and 17th Brazilian Power Electronics Conference (SPEC/COBEP)*, pp. 1–5, 2023, doi:10.1109/SPEC56436.2023.10407796.
- [15] A. Yazdani, R. Iravani, *Voltage-sourced converters in power systems: modeling, control, and applications*, John Wiley & Sons, 2010.
- [16] J. M. S. Callegari, R. R. Bastos, A. F. Cupertino, D. I. Brandao, H. A. Pereira, “Assessment of voltage detection-based Selective Harmonic Current Compensation Strategies for Different Non-linear Load Signatures”, *Eletrônica de Potência*, vol. 29, p. e202425, Aug. 2024, doi:10.18618/REP.2005.2.053060, URL: <https://journal.sobraep.org.br/index.php/rep/article/view/936>.
- [17] R. Cvetanovic, I. Z. Petric, P. Mattavelli, S. Buso, “Accurate High-Frequency Modeling of the Input Admittance of PWM Grid-Connected VSCs”, *IEEE Transactions on Power Electronics*, vol. 37, no. 9, pp. 10534–10545, 2022, doi:10.1109/TPEL.2022.3171611.
- [18] K. Ogata, *Modern control engineering fifth edition*, Pearson, 2010.
- [19] H. Akagi, E. Watanabe, M. Aredes, *Instantaneous Power Theory and Applications to Power Conditioning*, IEEE Press Series on Power and Energy Systems, Wiley, 2017.
- [20] R. W. Erickson, D. Maksimović, *Fundamentals of Power Electronics*, 3 ed., Springer Nature Switzerland AG, 2020.
- [21] S. Bacha, I. Munteanu, A. I. Bratcu, et al., “Power electronic converters modeling and control”, *Advanced textbooks in control and signal processing*, vol. 454, p. 454, 2014.
- [22] M. A. Ebrahim, B. A. Aziz, M. N. Nashed, F. A. Osman, “Optimal design of proportional-resonant controller and its harmonic compensators for grid-integrated renewable energy sources based three-phase voltage source inverters”, *IET Generation, Transmission & Distribution*, vol. 15, no. 8, pp. 1371–1386, 2021, doi:10.1049/gtd2.12108.

BIOGRAPHIES

André G. P. Alves was born in Rio de Janeiro, Brazil, in 1991. Graduated in Electrical Engineering at Universidade Federal do Rio de Janeiro (UFRJ) in 2016, receiving the top grade student title. Received the M.Sc. degree in Electrical Engineering at COPPE/UFRJ in 2018 and the D.Sc. degree at the same institution in 2022. Currently, he works as an assistant professor at Universidade do Estado do Rio de Janeiro (UERJ). His research is based in renewable energy resources applied to distributed generation systems, microgrids, HVDC systems and associated controls.

Laís F. C. Proença was born in Niterói, RJ, Brazil, in 1990. Graduated in Electronic and Computing Engineering at Universidade Federal do Rio de Janeiro (UFRJ) in 2014, receiving the top grade student title. Received the M.Sc. degree in Electrical Engineering at COPPE/UFRJ in 2017 and

the D.Sc. degree at the same institution in 2021. Currently, she works as an assistant professor at Universidade Federal do Rio de Janeiro (UFRJ). Her research is based in power electronics applied to distributed generation systems, microgrids, HVDC systems and associated controls.

Marcello Neves was born in Rio de Janeiro, RJ, Brazil, in 1992. He graduated in Electrical Engineering at Federal University of Rio de Janeiro (UFRJ) in 2016. He received the M.Sc. degree in Electrical Engineering at COPPE/UFRJ in 2018. Currently, he works as an assistant professor at the Federal Center of Technological Education Celso Suckow da Fonseca (CEFET/RJ). His research interests include renewable energy resources, battery energy storage systems, power electronics applied to power systems and embedded control systems.

Cleiton M. Freitas was born in Nilópolis, RJ, Brazil, in 1985. Graduated in Electrical Engineering with an emphasis in Electronics Systems at Rio de Janeiro State University (UERJ) in 2011. Received the M.Sc. degree in Electronics Engineering at PEL/UERJ in 2014 and the D.Sc. degree in Electrical Engineering at COPPE/UFRJ in 2020. Currently, he is an Adjunct Professor at Rio de Janeiro State University. His current research interests include Modular Multilevel Converter and its analytical modeling, grid-forming converters, renewable resources, and stability analysis of power electronics converters.

Luís G. B. Rolim was born in Niterói, Brazil, in 1966. He received the B.Sc. and M.Sc. degrees from the Federal University of Rio de Janeiro (UFRJ), Rio de Janeiro, Brazil, in 1989 and 1993, respectively, and the Dr.-Ing. degree from the Technical University Berlin, Berlin, Germany, in 1997 all in electrical engineering. Since 1990, he has been a Faculty Member of the Department of Electrical Engineering, Escola Politécnica, UFRJ, where he teaches and conducts research on power electronics, drives, and microprocessor control. He authored more than 50 papers published in Brazilian and international technical journals and conference proceedings. Dr. Rolim is a member of the Power Electronics Research Group at COPPE/UFRJ.

Robson F. S. Dias received the B.Sc. degree from UFPA in 2002 and the D.Sc. degree from UFRJ in 2008, both in electrical engineering. From 2009 to 2010, he was with CAPE at the University of Toronto, Canada, as a postdoctoral fellow. Currently, he is an associate professor at UFRJ. His areas of interest are Power Electronics, FACTS Device Application, Renewable Energy Resources, Real-Time Simulation, and Co-Simulation.